Original Article

Evaluating white matter alterations in Parkinson's disease-related *parkin* S/N167 mutation carriers using tract-based spatial statistics

Jinqiu Yu[1,2,3,4#], Lina Chen[1,3,4#], Guoen Cai[1,3,4], Yingqing Wang[1,3,4], Xiaochun Chen[1,3,4], Weimin Hong[2*], Qinyong Ye[1,3,4*]

[1]Department of Neurology, Fujian Institute of Geriatrics, Fujian Medical University Union Hospital, Fuzhou, China; [2]Department of Neurology, Affiliated Sanming First Hospital, Fujian Medical University, Sanming, China; [3]Institute of Neuroscience, Fujian Key Laboratory of Molecular Neurology, Fuzhou, China; [4]Institute of Clinical Neurology, Fujian Medical University, Fuzhou, China

Contributions: (I) Conception and design: Q Ye; (II) Administrative support: Q Ye, W Hong, X Chen; (III) Provision of study materials or patients: J Yu, G Cai; (IV) Collection and assembly of data: J Yu, L Chen; (V) Data analysis and interpretation: L Chen, Y Wang; (VI) Manuscript writing: All authors; (VII) Final approval of manuscript: All authors.

[#]These authors contributed equally to this work.

[*]These authors are joint last authors.

Correspondence to: Qinyong Ye. Department of Neurology, Fujian Institute of Geriatrics, Fujian Medical University Union Hospital. 29 Xinquan Road, Fuzhou 350001, China. Email: unionqyye@163.com; Weimin Hong. Department of Neurology, Affiliated Sanming First Hospital, Fujian Medical University, 29 Liedong Street, Sanming 365000, China. Email: 76128618@qq.com.

Background: Genetic susceptibility plays an important role in the pathogenesis of Parkinson's disease (PD). *parkin* S/N167 mutations may increase the risk of PD and affect white matter fibers in the brain. This cross-sectional study explored the effects of gene polymorphisms on white matter fiber damage in PD.

Methods: In all, 54 cases were enrolled in the study, including PD patients carrying *parkin* gene S/N167 mutations (G/A), PD patients without gene S/N167 mutations (G/G), and healthy controls (HC). The whole-brain white matter fiber skeleton was analyzed using the tract-based spatial statistics (TBSS) method. Two-way analysis of variance (ANOVA) and post hoc tests were used for data analyses.

Results: Two classification methods were used; one was based on disease classification, with 26 patients in the PD group (n=12 G/G, n=14 G/A) and 28 in the HC group (n=15 G/G, n=13 G/A), and the other was based on genetic classification, with 27 patients in the G/G group and 27 in the G/A group. In the G/A group, there was a wide range of significant changes in fractional anisotropy (FA), radial diffusivity (RD), and mean diffusivity (MD) values ($P<0.05$). There was also a significant decrease in FA in the PD-G/A group compared with the PD-G/G and HC-G/A groups ($P<0.05$).

Conclusions: There were more extensive brain white matter fiber damage and changes in PD patients; the G/A polymorphism may cause more extensive brain white matter damage.

Keywords: Diffusion tensor imaging (DTI); *parkin* gene S/N 167 polymorphism; Parkinson's disease (PD); white matter alteration

Submitted Oct 11, 2021. Accepted for publication May 05, 2022.
doi: 10.21037/qims-21-1007
View this article at: https://dx.doi.org/10.21037/qims-21-1007

Introduction

Parkinson's disease (PD) is the second most common neurodegenerative disorder, affecting approximately 1% of the global population aged >60 years (1-3). Genetic susceptibility plays an important role in the pathogenesis of PD, and family linkage analysis and mutation detection have confirmed that *parkin* gene is an important genetic pathogenic factor leading to PD (4). The *parkin* gene is the most common causative gene in Chinese patients with sporadic early-onset PD, and notably, exon deletion was the most common type of mutation (5). With advances in research, the role of *parkin* mutations in the onset of sporadic and late-onset PD patients has also received attention. Polymorphisms of S/N167 at the genotype and allele levels may increase the risk of PD (2,6). Within a cohort of 278 families, *parkin* mutations were identified in 11.2% of cases (50/448) with PD onset at >50 years of age (7). Due to the G to A mutation in exon 4 of the *parkin*, the serine (S) of the 167th codon is replaced by asparagine (N), thus forming the S/N167 polymorphism that may result in insufficient parkin protein production or insufficient activity of parkin protein (2,5,8).

Imaging genetics is a new discipline that links imaging and genetics to explore the effects of genetic variation on brain structure and function (9-12). Diffusion tensor imaging (DTI) technology has been widely used in the field of neurology in investigations of Alzheimer's disease, PD, and multiple sclerosis (12-14). White matter fibers transmit essential cerebral nerve impulses. There is evidence that the frontal and occipital lobes of patients with early PD may have extensive white matter microstructural damage, leading to changes in brain morphology and a series of clinical symptoms, such as motor and non-motor symptoms (15). The DTI method quantifies the amount and direction of diffused water molecules to reflect the spatial directivity and integrity of the structure of brain white matter and uses the fiber-tracking technique for three-dimensional reconstruction, which then intuitively reflects the trend, loss, and density of fasciculi in the white matter. This can then be used to estimate the integrity of the axons and the extent of microstructural damage (16). Tract-based spatial statistics (TBSS) is an automated whole-brain analysis method based on the white matter fiber skeleton that has recently been developed and become popular in white matter studies. The TBSS is a common alignment method based on fasciculi and can automatically and accurately analyze data from DTI (16,17). The most commonly used DTI parameters include fractional anisotropy (FA), radial diffusivity (RD), axial diffusivity (AD), and mean diffusivity (MD).

The FA values are primarily used to measure the isotropic diffusion ability of water molecules in the tissue and to characterize the directional distribution of the random movement of water molecules. A decrease in FA values may be due to demyelination, axon loss, or changes in axon size, and indicates that the arrangement of white matter fiber bundles is not regular and has lost integrity (18,19). The MD parameter is primarily used to describe the unidirectional diffusion capacity of water molecules in organic tissue and represents the overall movement trend of water molecules. Increased MD values indicate a poor capacity to retain water molecules in tissues, indicating tissue degradation (19). Meanwhile, TBSS can accurately align the major white matter tracts (17-20). It accurately positions the white matter through a white matter skeleton-based registration method and can quantitatively observe changes in the brain white matter diffusion index in patients. Thereby, TBSS can effectively reduce the image distortion caused by registration and smoothing (10,17), and has high sensitivity, objectivity, and interpretability in evaluating white matter fiber bundle damage (17).

In the present study, we explored differences in the white matter between PD and healthy control (HC) groups, as well as between patients carrying a *parkin* S/N167 mutation (G/A) and those not carrying the mutation (G/G), and analyzed the correlations between white matter fiber damage and PD cognition or motor function in patients. Our aims were to understand the pathological process of PD, to explore the effects of gene polymorphisms on white matter fiber damage in PD, and to provide more evidence for the disease mechanism in PD using genetic imaging. We present the following article in accordance with the STROBE reporting checklist (available at https://qims.amegroups.com/article/view/10.21037/qims-21-1007/rc).

Methods

Study design

This cross-sectional study included 54 participants was conducted in accordance with the Declaration of Helsinki (as revised in 2013). The study was approved by the Institutional Ethics Committee of Fujian Medical University Union Hospital, and all patients provided written informed consent. The flow diagram of inclusion process for PD and HC group presented in Figure S1.

Patients with PD included in this study were of Asian descent and were recruited from Fujian Medical University Union Hospital (Fujian, China) between March 2018 and December 2019. All patients underwent *parkin* S/N167 nucleotide polymorphism screening and head magnetic resonance imaging (MRI) examinations [including 3-dimensional brain volume (3D-BRAVO) and DTI imaging]. We included PD patients with the *parkin* S/N167 mutation (G/A) in the study and matched them for gender, age, number, and genotype with PD patients without the S/N167 mutation (G/G). We also recruited age- and gender-matched healthy controls (HC), including both G/A and G/G carriers, from the ShangDu Community. None of the control participants had a history or signs of neurological disorders.

Inclusion criteria

The PD patients enrolled in this study were clinically diagnosed according to the MDS clinical diagnostic criteria for Parkinson's disease (2015 edition) by two senior attending physicians (Qinyong Ye, Guoen Cai) who had received training before evaluating patients. All patients had received levodopa (L-DOPA) therapy and/or dopamine agonists on a regular basis and were taking their recommended PD drugs during the clinical evaluation. In addition, to be eligible for inclusion in this study, PD patients had to have an age of onset of >50 years and no family history of PD.

Exclusion criteria

Patients meeting any of the following criteria were excluded from the study:

(I) A clear history of brain diseases (including cerebrovascular disease, trauma, infection, poisoning, and autoimmune diseases) or obvious abnormalities in intracranial MRI (including obvious brain atrophy);
(II) Various secondary parkinsonian and parkinsonian-superimposed syndromes;
(III) Severe dementia, psychiatric diseases, neurodevelopmental diseases, anxiety, and depression;
(IV) Severe complications of diabetes and hypertension (e.g., cerebrovascular atherosclerosis, small cerebrovascular disease) that may affect the structural integrity of the brain white matter;
(V) Heavy consumption of tobacco and alcohol;
(VI) A history of exposure to heavy metals and other harmful substances;
(VII) Incomplete data, including for genetic tests, DTI, and clinical evaluations.

Clinical evaluation

All patients were clinically evaluated by neurology specialists. Cognitive function in the HC group was evaluated using the Mini-Mental State Examination (MMSE) (21). For PD patients, cognitive function was evaluated using the MMSE, the Montreal Cognitive Assessment (MoCA)-Changsha version (22), whereas motor symptoms were evaluated using Hoehn-Yahr scale (H-Y) and the Parkinson's Disease Unified Rating Scale Part III (UPDRS-III) (23).

Parkin genetic testing

Venous blood from the elbow of all participants was taken for detection of *parkin* S/N167 single nucleotide polymorphisms. The main reagent, Prime STAR HS (Premix), was purchased from Baori Medical Technology (Beijing, China) and the *parkin* gene S/N167 primers were synthesized by Inventec Trading (Shanghai, China). Sanger method sequencing was used, which included preparation of a reaction mixture (50 μL) containing 1 μL upstream primer (10 μM), 1 μL downstream primer (10 μM), 25 μL Prime STAR HS (Premix), 5 μL human genome DNA (5 ng/μL), and 18 μL ultrapure water. The amplified products were sent to Sangon Bioengineering (Shanghai, China) for Sanger DNA sequencing to determine gene polymorphisms.

MRI and image acquisition

Imaging data were acquired by a GE 3.0T dual-gradient MR scanner (GE Healthcare, Chicago, IL, USA). We used the 3D-BRAVO sequence to collect high-resolution T_1-weighted brain structure imaging data. The parameter settings were as follows: repetition time (TR) =8.7 ms, echo time (TE) =3.42 ms, flip time (TI) =400 ms, flip angle (FA) =12°, matrix =256×256, field of view (FOV) =240×240 mm, layer number =180, and slice thickness =1.1 mm. The DTI scan uses a spin-echo planar imaging [echo-planar imaging (EPI)] sequence to perform brain imaging, and echo-planar sequences in axial sections with the following settings: TR

=6,000 ms, TE =65.7 ms, FA =90°, matrix =128×128, field of view =240×240 mm, layer number =55, and layer thickness =3 mm (continuous scanning without spacing) in 16 non-linear diffusion-sensitive gradient directions with b values of 0 and 1,000 s/mm^2.

Image processing

The TBSS toolkit in FSL software (FMRIB Software Library, FMRIB, Oxford, UK) was used to construct a single FA image from the white matter skeleton for each participant (18). The TBSS toolkit uses a fitted tensor model to analyze the original diffusion data, registers the FA data of all cases into the standard space through a non-linear registration algorithm, creates an average FA skeleton, and normalizes the FA of each case. The threshold of the skeleton was set to 0.2 and the universal general linear model (Glm) is designed with age and gender as covariates. The TBSS framework with non-parametric permutation testing (5,000 permutations) was used for multiple comparisons correction and threshold-free cluster enhancement (TFCE). The results were considered significant at P<0.05(two-sided) for TFCE-corrected multiple comparisons. Brain regions with statistically significant differences between two groups on TBSS analysis were chosen as the brain regions of interest. Results were displayed as images superimposed on the MNI (Montreal Neurological Institute, Montreal, QC, Canada) template. Then, different brain regions were cut based on different white matter fibers referring to the Johns Hopkins University WM atlas (JHU-ICBM-DTI-81) distributed by FSL, and the mean FA values were extracted for statistical analysis. Brain regions that did not differ significantly were not extracted. MD, AD, and RD values were extracted using the same as the methods as used to extract FA values. The names of fiber bundles extracted were presented in Table S1.

Statistical analysis

Case data were analyzed using IBM SPSS 25.0 (IBM Corp., Armonk, NY, USA). The normality of data distribution was tested using the Shapiro-Wilk test (W test). Measurement data with a normal distribution and uniform variance, as well as data from two independent samples, were compared using independent sample *t*-tests, and measurement data are presented as the mean ± SD. Whereas measurement or grade data that did not have a normal distribution and or uniform variance were compared using the rank-sum test, and data are described with median (interquartile range). Two-way analysis of variance (ANOVA) was used to detect interactions between disease factors and genetic factors with built-in post hoc tests. Bonferroni tests were used to assess between-group differences. Pearson correlation analysis was used to calculate correlations between DTI parameters (FA, RD, MD, AD) of the PD group and the MMSE, MoCA, and UPDRS-III scores and H-Y classification. The false discovery rate (FDR) correction approach was used to correct for these correlations. Differences were considered statistically significant at P<0.05.

Results

Clinical variables

Of the 112 PD patients and 125 HCs invited to take part in the study, 54 were eligible for inclusion. Two classification methods were used; one was based on disease classification, with 26 patients in the PD group (12 G/G, 14 G/A) and 28 in the HC group (15 G/G, 13 G/A), and the other was based on genetic classification, with 27 in the G/G group and 27 in the G/A group. There were no significant differences in gender, age, or MMSE scores among the groups (*Tables 1,2*; Table S2).

TBSS analysis

Two-way ANOVA was performed based using disease and genetic factors as independent variables, and age and gender as covariates; no interaction effects were found on FA, MD, RD, or AD values (P<0.05). Group pairwise comparisons were then performed to compare the independent effects. *Figure 1A* shows FA values in brain regions of the PD and HC groups. As shown in *Figure 1B*, there were significant differences in FA values between the GG and GA groups.

Comparison of PD and HC groups

Significantly increased MD and RD and significantly decreased FA values were observed in numerous subcortical brain regions of the PD group compared with the HC group (*Figures 1A,2*, *Table 3*; Tables S3-S5). Specifically, lower FA values were seen in the PD compared with the HC group in the bilateral anterior corona radiata, bilateral anterior limb of the internal capsule, bilateral external capsules, bilateral posterior corona radiata, bilateral superior corona radiata,

Table 1 Demographic and behavioral characteristics of the included participants for HC and PD group

Characteristic	HC (n=28)	PD (n=26)	P
No. males	12	14	0.419[a]
Age	62.3±6	65.5±6.8	0.070[b]
MMSE	25.6±2.5	25±2.4	0.251[c]
Genotype (n)			
G/G	15	12	
G/A	13	14	
MoCA	–	20.2±3.1	
H-Y (%)	–		–
1.5		3.8	
2		34.6	
2.5		50	
3		11.5	
UPDRS-III	–	33.6±9.3	–

Age, Mini-Mental State Examination (MMSE) scores, and Montreal Cognitive Assessment (MoCA) scores are given as the mean ± SD. [a], Chi-square test; [b], independent sample *t*-test; c, Mann-Whitney U test. HC, healthy control; PD, Parkinson's disease; G/G, patients without parkin gene S/N167 mutations; G/A, patients carrying parkin gene S/N167 mutations; H-Y, Hoehn-Yahr Stage; UPDRS-III, Unified Parkinson's Disease Rating Scale Part III.

Table 2 Demographic and behavioral characteristics of the included participants for G/G and G/A group

Characteristic	G/G (n=27)	G/A (n=12)	P
No. males	14	12	0.586[a]
Age	63.9±6.6	63.8±6.6	0.951[b]
MMSE	25.6±2.4	25±2.5	0.416[c]

Unless indicated otherwise, data are given as the mean ± SD. [a], Chi-square test; [b], independent sample *t*-test; [c], Mann-Whitney U test. G/G, no S/N167 mutation; G/A, carrier of the S/N167 mutation; MMSE, Mini-Mental State Examination.

corpus callosum, and right posterior thalamic radiation. Significantly (P<0.05) higher MD values were seen in the bilateral posterior corona radiata, bilateral superior corona radiata, and the right posterior thalamic radiation of the PD compared with HC group. In addition, significantly (P<0.05) higher RD values were seen in the bilateral anterior corona radiata, bilateral anterior limb of internal capsule, bilateral external capsules, bilateral posterior corona radiata, bilateral posterior thalamic radiation, bilateral superior corona radiata, and corpus callosum of the PD versus HC group.

Comparisons between the G/G and G/A groups

Significantly increased MD and RD and significantly

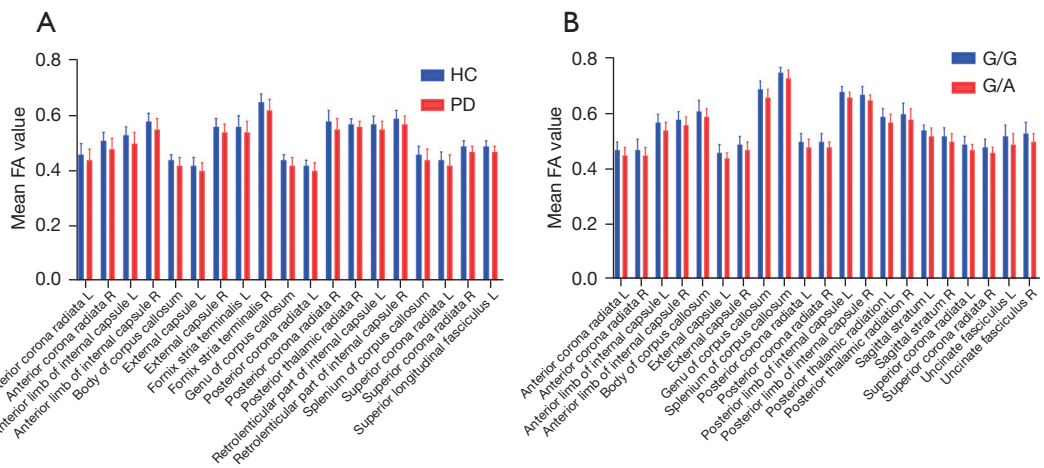

Figure 1 Brain regions showing significant differences in FA values: (A) PD versus HC; and (B) PD patients (G/A) versus PD patients (G/G). FA, fractional anisotropy; PD, Parkinson's disease; HC, healthy controls; G/G, patients without parkin gene S/N167 mutations; G/A, patients carrying parkin gene S/N167 mutations.

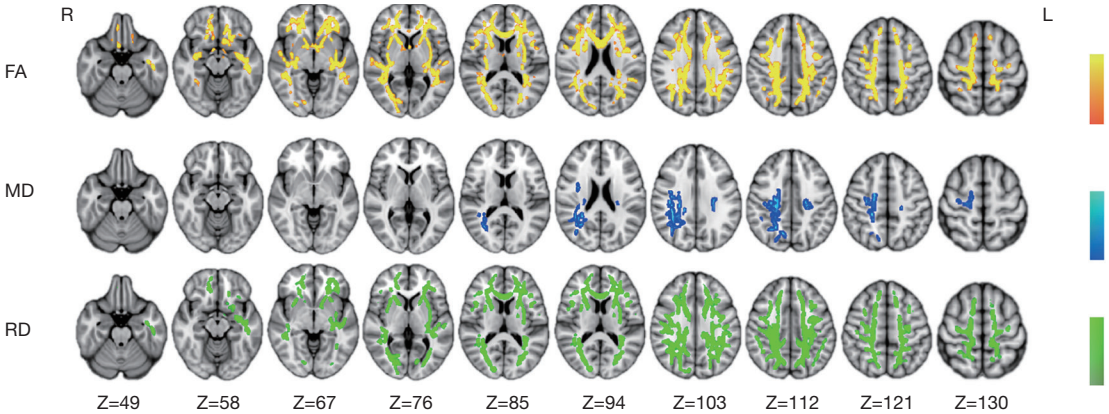

Figure 2 Comparison of diffusion tensor imaging indices (FA, MD, RD) between HC and patients with PD. Significant differences are indicated by the yellow regions overlaid on the mean FA skeleton, the blue regions overlaid on the mean MD skeleton, and the green regions overlaid on the mean RD skeleton. L, left; R, right; FA, fractional anisotropy; MD, mean diffusivity; RD, radial diffusivity; HC, healthy controls; PD, Parkinson's disease.

Table 3 Tract-based spatial statistics analysis of diffusion tensor imaging indices between groups

Modality	Group comparisons	Anatomical region
FA	HC > PD	acr-L, acr-R, alic-L, alic-R, Bcc, ec-L, ec-R, fst-L, fst-R, gcc, pcr-L, pcr-R, ptr-R, rlic-L, rlic-R, scc, scr-L, scr-R, slf-L
MD	HC < PD	pcr-L, pcr-R, ptr-R, scr-L, scr-R, slf-R
RD	HC < PD	acr-L, acr-R, alic-L, alic-R, bcc, ec-L, ec-R, fst-L, gcc, pcr-L, pcr-R, ptr-L, ptr-R, rpic-L, rpic-R, ss-L, scc, scr-L, scr-R, sfof-L
FA	G/G > G/A	acr-L, acr-R, alic-L, alic-R, boca, cp-L, cp-R, ccg-L, ct-L, ec-L, ec-R, fst-L, fst-R, gocc, icp-L, icp-R, ml-L, ml-R, mcp, pct, pcr-L, pcr-R, ploic-L, ploic-R, ptr-L, ptr-R, rpic-L, rpic-R, ss-L, ss-R, socc, scp-L, scr-L, scr-R, sfof, uf-L, uf-R
MD	G/G < G/A	acr-L, aloic-L, aloic-R, boca, cp-R, ct-R, ec-L, ec-R, fst-L, fst-R, ploic-L, ploic-R, ptr-R, rpic-L, rpic-R, ss-L, ss-R, scr-L, scr-R, slf-L
RD	G/G < G/A	acr-L, acr-R, aloic-L, aloic-R, boca, cp-L, cp-R, ct-L, ct-R, ec-L, ec-R, fst-L, goca, icp-R, ml-R, mcp, pct, pcr-L, pcr-R, ploic-L, ploic-R, ptr-L, ptr-R, rpoic-L, rpoic-R, ss-L, ss-R, soca, scr-L, scr-R, sfof-L, slf-L, slf-R, uf-R
FA	PD-G/G > PD-G/A	ct-L, ec-L, ec-R, fst-L, gocc, mcp, rpoic-L
FA	HC-G/G > HC-G/A	acr-L, cp-L, cp-R, mcp, ploc-L, ploc-R, scr-L, scr-R
MD	PD-G/G > PD-G/A	aloc-L, ct-R, ec-L, fst-L
MD	HC-G/G > HC-G/A	alic-L, alic-R, bocc, ct-R, scr-R
RD	PD-G/G > PD-G/A	aloic-L, cp-L, cp-R, ec-R, fst-L, gocc, rpoic-L
RD	HC-G/G > HC-G/A	cp-L, cp-R, icp-R, ploic-L, ploic-R

acr, anterior corona radiata; aloic, anterior limb of internal capsule; boca, body of the corpus callosum; ccg, cingulum cingulate gyrus; ch, cingulum hippocampus; cp, cerebral peduncle; ct, corticospinal tract; ec, external capsule; FA, fractional anisotropy; fst, fornix stria terminalis; G/G, patients without parkin gene S/N167 mutations; G/A, patients carrying parkin gene S/N167 mutations; goca, genu of the corpus callosum; HC, healthy control; icp, inferior cerebellar peduncle; L, left; mcp, middle cerebellar peduncle; MD, mean diffusivity; ml, medial lemniscus; pcr, posterior corona radiata; pct, pontine crossing tract; PD, Parkinson's disease; ploic, posterior limb of the internal capsule; ptr, posterior thalamic radiation; rpoic, retrolenticular part of the internal capsule; R, right; RD, radial diffusivity; scp, superior cerebellar peduncle; scr, superior corona radiata; sfof, superior fronto-occipital fasciculus; socc, splenium of the corpus callosum; ss, sagittal stratum; uf, uncinate fasciculus.

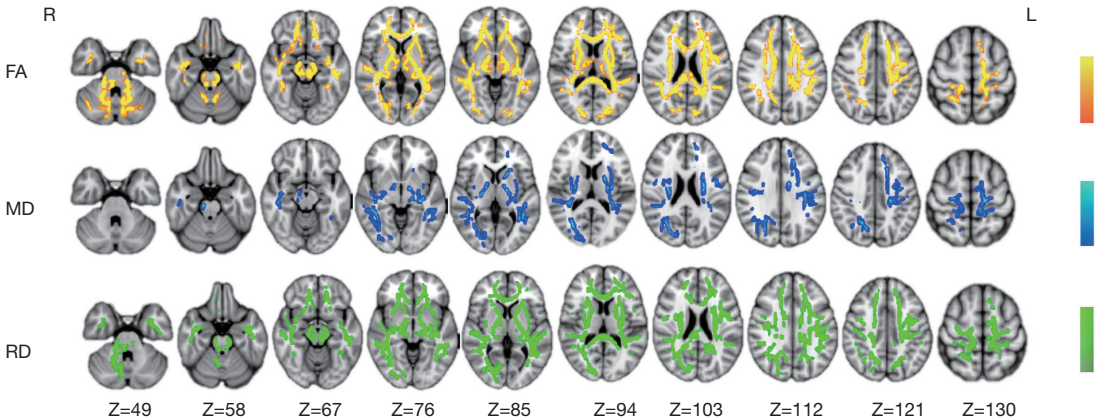

Figure 3 Comparison of diffusion tensor imaging indices (FA, MD, RD) between PD patients (G/A) and PD patients (G/G). Significant differences are indicated by the yellow regions overlaid on the mean FA skeleton, the blue regions overlaid on the mean MD skeleton, and the green regions overlaid on the mean RD skeleton. R, right L, left; FA, fractional anisotropy; MD, mean diffusivity; RD, radial diffusivity; G/A, patients carrying parkin gene S/N167 mutations; G/G, patients without parkin gene S/N167 mutations.

decreased FA values were observed in numerous subcortical brain regions of the G/A compared G/G group (*Figures 1B,3*, *Table 3*; Tables S6-S8). Specifically, FA values were lower in the G/A than G/G group in the bilateral anterior corona radiata, bilateral anterior limb of internal capsule, bilateral external capsules, bilateral posterior corona radiata, bilateral posterior limb of internal capsule, bilateral posterior thalamic radiation, bilateral sagittal stratum, bilateral superior corona radiata, and corpus callosum. These significant differences in white matter tracts between the G/G and G/A groups overlapped those seen between the PD and HC groups. There were also significant decreases in FA values in the bilateral uncinate fasciculus in the G/A group. There were increases in MD values in the G/A versus G/G group in the bilateral anterior limb of the internal capsule, bilateral external capsule, bilateral posterior thalamic radiation, bilateral sagittal stratum, and bilateral superior corona radiata. In addition, RD values were significantly ($P<0.05$) increased in the G/A versus G/G group in the bilateral anterior corona radiata, bilateral anterior limb of internal capsule, bilateral external capsules, bilateral posterior corona radiata, bilateral posterior thalamic radiation, bilateral superior corona radiata, and corpus callosum.

Comparisons within subgroups

PD-G/G versus PD-G/A

In the PD-G/A group, FA values in the corticospinal tract, bilateral external capsules, left fornix stria terminalis, genu of the corpus callosum, and middle cerebellar peduncle were significantly lower than in the PD-G/G group (*Figure 4*, *Table 3*; Table S9), whereas MD values in the left interior limb of the internal capsule, right corticospinal tract, and left external capsule were significantly higher in the PD-G/A group. RD values in the left anterior limb of the internal capsule, bilateral cerebral peduncle, left corticospinal tract, right external capsule, left fornix stria terminalis, genu of the corpus callosum, and left retrolenticular part of the internal capsule were significantly higher in the PD-G/A than PD-G/G group (*Figure 4*, *Table 1*; Tables S9-S11).

HC-G/G versus HC-G/A

The FA values in the bilateral posterior limb of the internal capsule, the left anterior limb of the internal capsule, the left posterior corona radiata, left external capsule, left anterior corona radiata, bilateral cerebral peduncle, middle cerebellar peduncle, bilateral posterior limb of the internal capsule, and bilateral superior corona radiata were significantly lower in the HC-G/A than HC-G/G group. In contrast, MD values in the bilateral anterior limb of the internal capsule, body of the corpus callosum, right corticospinal tract, and right superior corona radiata were significantly higher in the HC-G/A than HC-G/G group. The RD values were also significantly ($P<0.05$) higher in the HC-G/A than HC-G/G group in the bilateral cerebral peduncle, right inferior cerebellar peduncle, and bilateral posterior limb of the internal capsule (*Figure 4*, *Table 3*; Tables S12-S14).

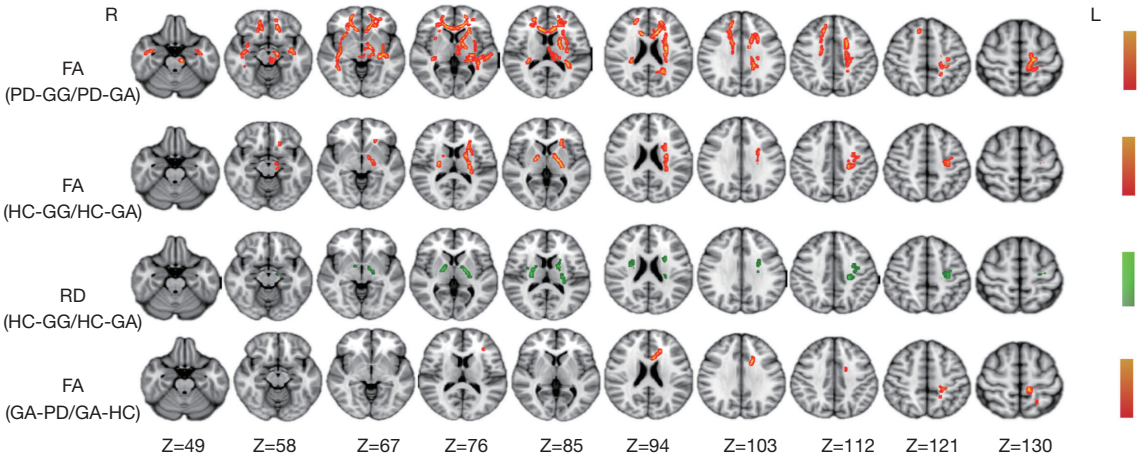

Figure 4 Comparison of diffusion tensor imaging indices (FA, RD) between groups. Significant differences are indicated by the red regions overlaid on the mean FA skeleton and the green regions overlaid on the mean RD skeleton. R, right; L, left; FA, fractional anisotropy; PD, Parkinson's disease; G/G, patients without parkin gene S/N167 mutations; G/A, patients carrying parkin gene S/N167 mutations; HC, healthy controls; RD, radial diffusivity.

G/A-HC versus G/A-PD

There were no significant differences between the G/A-PD and G/A-HC groups.

G/G-HC versus G/G-PD

There were no significant differences between the G/G-PD and G/G-HC groups.

Correlation analysis between the parameter values and clinical indicators of PD

The UPDRS-III scores were negatively correlated with FA values of the bilateral anterior corona radiata, bilateral external capsules, right fornix stria terminalis, splenium of the corpus callosum, and right superior corona radiata. There was a positive correlation between UPDRS-III scores and MD values of the bilateral superior corona radiata and the right superior longitudinal fasciculus, as well as between UPDRS-III scores and RD values of the bilateral anterior corona radiata, bilateral anterior limb of the internal capsule, bilateral external capsule, splenium of the corpus callosum, and bilateral superior corona radiata.

The MoCA scores were positively correlated with FA values of the bilateral anterior corona radiata, bilateral anterior limb of the internal capsule, body of the corpus callosum, bilateral external capsules, genu of the corpus callosum, and bilateral superior corona radiata. The MoCA scores were negatively correlated with RD values of the anterior limb of the internal capsule, bilateral external capsule, and body of the corpus callosum (*Tables 4-6*, *Figure 5*).

The MoCA scores were positively correlated with FA values of the left posterior corona radiata and the MD value of the right superior corona radiata (*Tables 4-6*).

Discussion

This study evaluated abnormalities in white matter tracts on diffusion-weighted MRI based on TBSS. Compared with the HC group, the PD group had extensive white matter fiber damage in many brain areas on the FA and RD maps. The difference in the MD map involved a smaller brain area. These findings are similar to those reported previously (9,14,24,25). Extensive areas of white matter fiber damage were found in the PD group, which may contribute to the diversity of PD clinical symptoms. Although ANOVA did not reveal a significant interaction between genotype and disease status, multiple comparisons revealed that there may be more pronounced damage in the G/A than in the G/G group. Similarly, there was serious damage in the G/A-PD compared with the G/G-PD group. However, there were no significant differences identified between the GG/HC and GG/PD groups. This suggests that the G/A polymorphism can cause more serious white matter fiber damage.

Some *parkin* mutations lead to the production of an abnormally small and non-functional parkin protein and cause functional defects of the parkin protein (5,26,27). The

Table 4 Clinical correlations of fractional anisotropy with white matter changes

Anatomical region	H-Y		UPDRS-III		MoCA		MMSE	
	r	P value	r	P value	r	P value	r	P value
Anterior corona radiata L	–0.107	0.603	–0.643	0.000	0.560	0.011	0.172	0.4
Anterior corona radiata R	–0.154	0.453	–0.538	0.013	0.456	0.022	–0.001	0.997
Anterior limb of internal capsule L	–0.281	0.164	–0.328	0.102	0.546	0.011	0.012	0.954
Anterior limb of internal capsule R	–0.323	0.107	–0.282	0.162	0.498	0.018	–0.09	0.66
Body of the corpus callosum	–0.269	0.183	–0.213	0.296	0.537	0.011	0.159	0.439
External capsule L	–0.083	0.686	–0.408	0.036	0.466	0.021	–0.133	0.518
External capsule R	–0.124	0.545	–0.410	0.036	0.481	0.02	–0.132	0.519
Fornix stria terminalis L	–0.151	0.462	–0.188	0.359	0.193	0.346	0.103	0.617
Fornix stria terminalis R	–0.247	0.224	–0.412	0.036	0.294	0.145	–0.071	0.729
Genu of the corpus callosum	–0.304	0.131	–0.251	0.216	0.531	0.011	0.108	0.599
Posterior corona radiata L	–0.022	0.915	–0.036	0.862	0.09	0.663	0.420	0.032
Posterior corona radiata R	–0.244	0.23	–0.204	0.319	0.204	0.318	–0.386	0.052
Posterior thalamic radiation R	–0.323	0.107	–0.321	0.109	0.331	0.098	–0.132	0.521
Retrolenticular part of internal capsule L	–0.257	0.206	–0.108	0.599	0.047	0.82	–0.275	0.174
Retrolenticular part of internal capsule R	–0.262	0.197	–0.284	0.16	0.25	0.218	–0.12	0.559
Splenium of the corpus callosum	–0.173	0.397	–0.391	0.036	0.326	0.104	–0.041	0.841
Superior corona radiata L	–0.181	0.375	–0.361	0.07	0.594	0.011	0.094	0.648
Superior corona radiata R	–0.204	0.319	–0.397	0.036	0.415	0.037	–0.086	0.677
Superior longitudinal fasciculus L	0.031	0.881	–0.249	0.22	0.21	0.304	–0.283	0.162

H-Y, Hoehn-Yahr Stage scale; L, left; MMSE, Mini-Mental State Examination; MoCA, Montreal Cognitive Assessment; R, right; UPDRS-III, Unified Parkinson's Disease Rating Scale Part III.

Table 5 Clinical correlations of mean diffusivity with white matter changes

Anatomical region	H-Y		UPDRS-III		MoCA		MMSE	
	r	P value	r	P value	r	P value	r	P value
Posterior corona radiata L	0.08	0.697	0.228	0.262	–0.033	0.875	0.278	0.169
Posterior corona radiata R	–0.059	0.776	0.382	0.054	–0.124	0.545	0.295	0.144
Posterior thalamic radiation R	–0.067	0.744	0.327	0.103	–0.117	0.57	0.241	0.235
Superior corona radiata L	0.129	0.528	0.544	0.013	0.1	0.626	0.343	0.086
Superior corona radiata R	0.026	0.899	0.447	0.023	–0.059	0.774	0.430	0.028
Superior longitudinal fasciculus R	–0.116	0.574	0.500	0.014	–0.104	0.612	0.376	0.058

H-Y, Hoehn-Yahr Stage scale; L, left; MMSE, Mini-Mental State Examination; MoCA, Montreal Cognitive Assessment; R, right; UPDRS-III, Unified Parkinson's Disease Rating Scale Part III.

Table 6 Clinical correlations of radial diffusivity with white matter changes

Anatomical region	H-Y		UPDRS-III		MoCA		MMSE	
	r	P value	r	P value	r	P value	r	P value
Anterior corona radiata L	–0.063	0.759	0.667	0.004	–0.377	0.058	0.171	0.404
Anterior corona radiata R	0.097	0.639	0.517	0.004	–0.510	0.008	0.121	0.557
Anterior limb of the internal capsule L	0.078	0.704	0.401	0.015	–0.452	0.021	0.09	0.663
Anterior limb of the internal capsule R	0.106	0.606	0.364	0.068	–0.438	0.025	–0.084	0.683
Body of the corpus callosum	–0.028	0.893	0.504	0.005	–0.457	0.019	0.263	0.195
External capsule L	0.045	0.827	0.522	0.004	–0.473	0.015	0.236	0.245
External capsule R	0.063	0.759	0.323	0.107	–0.236	0.246	0.025	0.902
Fornix stria terminalis L	0.143	0.486	0.299	0.138	–0.448	0.022	–0.047	0.821
Genu of the corpus callosum	–0.056	0.785	0.244	0.229	–0.036	0.862	0.377	0.058
Posterior corona radiata L	0.03	0.884	0.343	0.086	–0.152	0.458	0.334	0.095
Posterior corona radiata R	0.023	0.909	0.388	0.016	0.006	0.976	0.183	0.37
Posterior thalamic radiation L	0.198	0.333	0.359	0.072	–0.228	0.262	0.141	0.491
Posterior thalamic radiation R	0.181	0.377	0.176	0.391	–0.115	0.575	0.382	0.054
Retrolenticular part of the internal capsule L	0.091	0.658	0.311	0.122	–0.226	0.268	0.191	0.351
Retrolenticular part of the internal capsule R	0.109	0.598	0.399	0.015	–0.283	0.161	0.038	0.854
Sagittal stratum L	0.089	0.664	0.561	0.004	–0.273	0.177	0.241	0.236
Splenium of the corpus callosum	0.054	0.793	0.535	0.004	–0.258	0.203	0.298	0.139
Superior corona radiata L	–0.125	0.544	0.383	0.054	–0.159	0.438	–0.052	0.8
Superior corona radiata R	–0.118	0.565	0.341	0.089	–0.024	0.909	0.116	0.574
Superior fronto-occipital fasciculus L	–0.054	0.795	0.460	0.008	–0.088	0.669	0.374	0.06

H-Y, Hoehn-Yahr Stage scale; L, left; MMSE, Mini-Mental State Examination; MoCA, Montreal Cognitive Assessment; R, right; UPDRS-III, Unified Parkinson's Disease Rating Scale Part III.

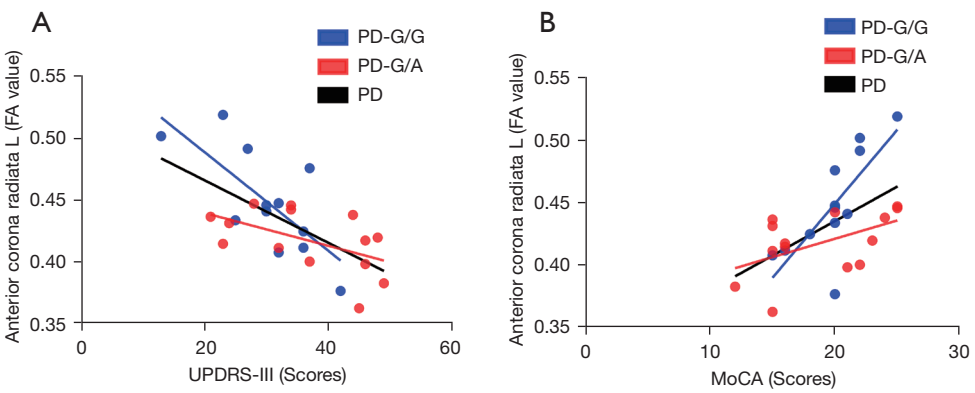

Figure 5 Correlation between FA values of the anterior corona radiata left and (A) UPDRS-III and (B) MoCA scores. FA, fractional anisotropy; PD, Parkinson's disease; G/G, patients without parkin gene S/N167 mutations; G/A, patients carrying parkin gene S/N167 mutations; UPDRS-III, Unified Parkinson's Disease Rating Scale Part III; MoCA, Montreal Cognitive Assessment.

parkin protein may function similarly to ubiquitin family members, and defects in the parkin protein in autosomal recessive juvenile parkinsonism may interfere with the ubiquitin-mediated proteolytic pathway leading to the death of neurons in the nigra (28). This causes intracellular protein metabolism disorders, the accumulation of toxic substrates, and ultimately cell death, or disrupts normal cell activities, such as the synthesis and release of dopamine synaptic vesicles. Therefore, the *parkin* S/N167 polymorphism may disrupt expression of the parkin protein, leading to the onset of PD and affecting the clinical symptoms of PD. To a certain extent, we can speculate that this genetic polymorphism can increase the risk of PD onset and affect disease progression (5).

No significant differences were found between the G/G-PD and the G/G-HC groups. This may be due to the milder damage to the white matter tracts in the G/G-PD group. However, it may also be due to the small sample size of the two groups. Based on FA maps, compared with the G/A-HC group, the G/A-PD group had more severe damage in the left brain. This may be related to the laterality of PD, with the left cerebral hemisphere, which is more closely related to primary brain networks such as movement and sensory networks, being the predominantly affected hemisphere. Then, the occurrence of clinical symptoms is more strongly related to the degree of damage in the left cerebral hemisphere (29).

The UPDRS-III and MoCA scores of the PD group were significantly correlated with FA, MD, and RD values of the white matter fibers in multiple, significantly different brain regions compared with the HC group. The white matter fibers related to cognitive function include the corpus callosum and peduncles, the anterior, superior, and posterior corona radiatas, and the external capsule. Those related to movement are the corpus callosum and compression, anterior and superior corona radiata, external capsule, forelimb of the internal capsule, and superior longitudinal tract.

Sisti *et al.* (25) found that cognitive decline is not only related to lesions in local brain regions, but may also be related to the destruction of white matter fibers and impaired connection function associated with these brain regions. Information transfer between two regions is transformed, and this plays an important role in the formation and retrieval of memories, as well as in the process of cognition (22,30). It is also related to cognitive impairment, such as in affective disorder and executive function (18).

The corona radiata connects the internal capsule and the ipsilateral cerebral cortex, including the premotor area, the motor center, and the sensory center. There is also a close connection between the corona radiata and cognitive function (31). The anterior corona radiata is connected to the prefrontal lobe and affects cognitive function through the prefrontal lobe–basal ganglia loop. Researchers have found that white matter lesions play an important role in cognitive decline (19,32,33). Patients with PD who have white matter lesions have a higher risk of developing cognitive dysfunction, and the severity of destruction of brain white matter fiber integrity is closely related to the severity of cognitive dysfunction in PD patients (34). The anterior limb of the internal capsule is related to the connection function of the thalamus, pons, and frontal lobe, and is closely associated with the functions of cognitive processing, emotion, and motivational decision-making (35). The external capsule is mainly comprised of cortical tegmental fibers and cortical striatal fibers that are sent from the insula to the midbrain and hypothalamus (24). The impaired mobility of PD patients is related to a decline in their ability to perceive the outside world (36). Through a series of complex brain network connections, external capsule lesions can affect cognitive function and movement ability through functional connections of striatal or visual pathways. Some studies have found that the fibers connecting the temporal and occipital lobes, such as the superior longitudinal fasciculus, are also related to decreased exercise capacity and impairments in goal-oriented behavior (24,37,38). A study on freezing gait (39) found that it is related not only to damage to motor fibers, such as the corticospinal tract and cerebrum, but also to damage to the superior longitudinal tract.

A mouse PD model showed that after 1-methyl-4-phenyl 1-1,2,3,6-tetrahydropyridine (MPTP) intoxication, cell loss in brain regions involved in pathology reflects reduced FA in white matter projections in these regions (40). The decrease in FA indicates the loss of white matter integrity due to the destruction of the directed axonal membrane, whereas the increase in MD reflects the reduced membrane density that hinders diffusion (15).

In the present study, TBSS analysis revealed that the white matter fibers of many brain areas related to movement and cognition in PD patients were damaged. The FA map revealed lower FA values in many white matter brain areas in the PD-G/A group, suggesting that PD patients with point mutations in the *parkin* S/N167 gene (G/A) have more severe brain white matter fiber damage,

which may indicate disruption of white matter fibers that, in turn, affects fiber connectivity, causing motor function and cognitive dysfunction.

Limitations

This study had some limitations. First, this was a single-center study, and all participants were Asian. Future multicenter, multi-ethnic cohort studies are needed to reduce bias due to case inclusion. Second, there is the potential for paradoxically significant results to emerge after splitting the dataset in multiple ways. Finally, this study was a cross-sectional study with a small sample size; a prolonged cohort study is needed to further explore the relevant effects of *parkin* S/N167 gene mutations.

Conclusions

There were more extensive brain white matter fiber damage and changes in PD patients compared with HCs, with the G/A polymorphism being associated with more extensive brain white matter damage. This study may provide more imaging information to reveal the etiology and pathogenesis of PD gene mutations. More longitudinal clinical studies are needed in the future to confirm our findings.

Acknowledgments

Funding: This work was supported by the Central Government Directs Special Funds for Local Science and Technology Development (No. 2019L301).

Footnote

Reporting Checklist: The authors have completed the STROBE reporting checklist. Available at https://qims.amegroups.com/article/view/10.21037/qims-21-1007/rc

Conflicts of Interest: All authors have completed the ICMJE uniform disclosure form (available at https://qims.amegroups.com/article/view/10.21037/qims-21-1007/coif). The authors have no conflicts of interest to declare.

Ethical Statement: The authors are accountable for all aspects of the work in ensuring that questions related to the accuracy or integrity of any part of the work are appropriately investigated and resolved. The study was conducted in accordance with the Declaration of Helsinki (as revised in 2013). This study was approved by the Institutional Ethics Committee of Fujian Medical University Union Hospital and all participants provided written informed consent.

References

1. Kalia LV, Lang AE. Parkinson's disease. Lancet 2015;386:896-912.
2. Dekker MC, Bonifati V, van Duijn CM. Parkinson's disease: piecing together a genetic jigsaw. Brain 2003;126:1722-33.
3. Grayson M. Parkinson's disease. Nature 2016;538:S1.
4. Zou H, Chen B, Peng X, Feng X, Dong X. A Meta-analysis of Parkin Gene S/N167 Polymorphism in the Risks of Parkinson's Disease. Chinese Journal of Evidence-Based Medicine 2004;4, 157-63.
5. Jiang Y, Yu M, Chen J, Zhou H, Sun W, Sun Y, Li F, Wei L, Pinkhardt EH, Zhang L, Yuan Y, Wang Z. Parkin is the most common causative gene in a cohort of mainland Chinese patients with sporadic early-onset Parkinson's disease. Brain Behav 2020;10:e01765.
6. Wasner K, Grünewald A, Klein C. Parkin-linked Parkinson's disease: From clinical insights to pathogenic mechanisms and novel therapeutic approaches. Neurosci Res 2020;159:34-9.
7. Foroud T, Uniacke SK, Liu L, Pankratz N, Rudolph A, Halter C, Shults C, Marder K, Conneally PM, Nichols WC; Parkinson Study Group. Heterozygosity for a mutation in the parkin gene leads to later onset Parkinson disease. Neurology 2003;60:796-801.
8. Mizuno Y, Hattori N, Mori H, Suzuki T, Tanaka K. Parkin and Parkinson's disease. Curr Opin Neurol 2001;14:477-82.
9. Guimarães RP, Campos BM, de Rezende TJ, Piovesana L, Azevedo PC, Amato-Filho AC, Cendes F, D'Abreu A. Is Diffusion Tensor Imaging a Good Biomarker for Early Parkinson's Disease? Front Neurol 2018;9:626.

10. Nigro P, Chiappiniello A, Simoni S, Paolini Paoletti F, Cappelletti G, Chiarini P, Filidei M, Eusebi P, Guercini G, Santangelo V, Tarducci R, Calabresi P, Parnetti L, Tambasco N. Changes of olfactory tract in Parkinson's disease: a DTI tractography study. Neuroradiology 2021;63:235-42.
11. Thaler A, Kliper E, Maidan I, Herman T, Rosenberg-Katz K, Bregman N, Gurevich T, Shiner T, Hausdorff JM, Orr-Urtreger A, Giladi N, Mirelman A. Cerebral Imaging Markers of GBA and LRRK2 Related Parkinson's Disease and Their First-Degree Unaffected Relatives. Brain Topogr 2018;31:1029-36.
12. Teipel SJ, Walter M, Likitjaroen Y, Schönknecht P, Gruber O. Diffusion tensor imaging in Alzheimer's disease and affective disorders. Eur Arch Psychiatry Clin Neurosci 2014;264:467-83.
13. Chen W, Lin H, Lyu M, Wang VJ, Li X, Bao S, Sun G, Xia J, Wang P; Alzheimer's Disease Neuroimaging Initiative†. The potential role of leukoaraiosis in remodeling the brain network to buffer cognitive decline: a Leukoaraiosis And Disability study from Alzheimer's Disease Neuroimaging Initiative. Quant Imaging Med Surg 2021;11:183-203.
14. Whitwell JL, Schwarz CG, Reid RI, Kantarci K, Jack CR Jr, Josephs KA. Diffusion tensor imaging comparison of progressive supranuclear palsy and corticobasal syndromes. Parkinsonism Relat Disord 2014;20:493-8.
15. Thaler A, Artzi M, Mirelman A, Jacob Y, Helmich RC, van Nuenen BF, Gurevich T, Orr-Urtreger A, Marder K, Bressman S, Bloem BR, Hendler T, Giladi N, Ben Bashat D; LRRK2 Ashkenazi Jewish Consortium. A voxel-based morphometry and diffusion tensor imaging analysis of asymptomatic Parkinson's disease-related G2019S LRRK2 mutation carriers. Mov Disord 2014;29:823-7.
16. Li XR, Ren YD, Cao B, Huang XL. Analysis of white matter characteristics with tract-based spatial statistics according to diffusion tensor imaging in early Parkinson's disease. Neurosci Lett 2018;675:127-32.
17. Wei X, Luo C, Li Q, Hu N, Xiao Y, Liu N, Lui S, Gong Q. White Matter Abnormalities in Patients With Parkinson's Disease: A Meta-Analysis of Diffusion Tensor Imaging Using Tract-Based Spatial Statistics. Front Aging Neurosci 2021;12:610962.
18. Burzynska AZ, Preuschhof C, Bäckman L, Nyberg L, Li SC, Lindenberger U, Heekeren HR. Age-related differences in white matter microstructure: region-specific patterns of diffusivity. Neuroimage 2010;49:2104-12.
19. Davis SW, Dennis NA, Buchler NG, White LE, Madden DJ, Cabeza R. Assessing the effects of age on long white matter tracts using diffusion tensor tractography. Neuroimage 2009;46:530-41.
20. Shang S, Wu J, Chen YC, Chen H, Zhang H, Dou W, Wang P, Cao X, Yin X. Aberrant cerebral perfusion pattern in amnestic mild cognitive impairment and Parkinson's disease with mild cognitive impairment: a comparative arterial spin labeling study. Quant Imaging Med Surg 2021;11:3082-97.
21. Folstein MF, Folstein SE, McHugh PR. "Mini-mental state". A practical method for grading the cognitive state of patients for the clinician. J Psychiatr Res 1975;12:189-98.
22. Jin H, Ding B, Yang X, Lei Z, Zeng X, Bai S, Tang X, Tu Q. Application of the Beijing version of MoCA in the ischemic cerebrovascular disease population in the Changsha region and the formation of the MoCA version in Changsha. Chinese Journal of Neuropsychiatric Diseases 2011;37:349-53.
23. Movement Disorder Society Task Force on Rating Scales for Parkinson's Disease. The Unified Parkinson's Disease Rating Scale (UPDRS): status and recommendations. Mov Disord 2003;18:738-50.
24. Haller S, Badoud S, Nguyen D, Garibotto V, Lovblad KO, Burkhard PR. Individual detection of patients with Parkinson disease using support vector machine analysis of diffusion tensor imaging data: initial results. AJNR Am J Neuroradiol 2012;33:2123-8.
25. Sisti HM, Geurts M, Gooijers J, Heitger MH, Caeyenberghs K, Beets IA, Serbruyns L, Leemans A, Swinnen SP. Microstructural organization of corpus callosum projections to prefrontal cortex predicts bimanual motor learning. Learn Mem 2012;19:351-7.
26. Kitada T, Asakawa S, Hattori N, Matsumine H, Yamamura Y, Minoshima S, Yokochi M, Mizuno Y, Shimizu N. Mutations in the parkin gene cause autosomal recessive juvenile parkinsonism. Nature 1998;392:605-8.
27. Reed X, Bandrés-Ciga S, Blauwendraat C, Cookson MR. The role of monogenic genes in idiopathic Parkinson's disease. Neurobiol Dis 2019;124:230-9.
28. Klionsky DJ, Abdelmohsen K, Abe A, Abedin MJ, Abeliovich H, Acevedo Arozena A, et al. Guidelines for the use and interpretation of assays for monitoring autophagy (3rd edition). Autophagy 2016;12:1-222.
29. Mellick GD, Buchanan DD, Hattori N, Brookes AJ, Mizuno Y, Le Couteur DG, Silburn PA. The parkin gene S/N167 polymorphism in Australian Parkinson's disease patients and controls. Parkinsonism Relat Disord 2001;7:89-91.

30. Peltier J, Roussel M, Gerard Y, Lassonde M, Deramond H, Le Gars D, De Beaumont L, Godefroy O. Functional consequences of a section of the anterior part of the body of the corpus callosum: evidence from an interhemispheric transcallosal approach. J Neurol 2012;259:1860-7.
31. Huang X, Du X, Song H, Zhang Q, Jia J, Xiao T, Wu J. Cognitive impairments associated with corpus callosum infarction: a ten cases study. Int J Clin Exp Med 2015;8:21991-8.
32. Wang J, Liang Y, Chen H, Wang W, Wang Y, Liang Y, Zhang Y. Structural changes in white matter lesion patients and their correlation with cognitive impairment. Neuropsychiatr Dis Treat 2019;15:1355-63.
33. Yu J, Lam CLM, Lee TMC. White matter microstructural abnormalities in amnestic mild cognitive impairment: A meta-analysis of whole-brain and ROI-based studies. Neurosci Biobehav Rev 2017;83:405-16.
34. Chen YS, Chen MH, Lu CH, Chen PC, Chen HL, Yang IH, Tsai NW, Lin WC. Associations among Cognitive Functions, Plasma DNA, and White Matter Integrity in Patients with Early-Onset Parkinson's Disease. Front Neurosci 2017;11:9.
35. Abraham A, Hart A, Andrade I, Hackney ME. Dynamic Neuro-Cognitive Imagery Improves Mental Imagery Ability, Disease Severity, and Motor and Cognitive Functions in People with Parkinson's Disease. Neural Plast 2018;2018:6168507.
36. Safadi Z, Grisot G, Jbabdi S, Behrens TE, Heilbronner SR, McLaughlin NCR, Mandeville J, Versace A, Phillips ML, Lehman JF, Yendiki A, Haber SN. Functional Segmentation of the Anterior Limb of the Internal Capsule: Linking White Matter Abnormalities to Specific Connections. J Neurosci 2018;38:2106-17.
37. Conner AK, Briggs RG, Sali G, Rahimi M, Baker CM, Burks JD, Glenn CA, Battiste JD, Sughrue ME. A Connectomic Atlas of the Human Cerebrum-Chapter 13: Tractographic Description of the Inferior Fronto-Occipital Fasciculus. Oper Neurosurg (Hagerstown) 2018;15:S436-43.
38. Shin J, Rowley J, Chowdhury R, Jolicoeur P, Klein D, Grova C, Rosa-Neto P, Kobayashi E. Inferior Longitudinal Fasciculus' Role in Visual Processing and Language Comprehension: A Combined MEG-DTI Study. Front Neurosci 2019;13:875.
39. Canu E, Agosta F, Sarasso E, Volontè MA, Basaia S, Stojkovic T, Stefanova E, Comi G, Falini A, Kostic VS, Gatti R, Filippi M. Brain structural and functional connectivity in Parkinson's disease with freezing of gait. Hum Brain Mapp 2015;36:5064-78.
40. Vaillancourt DE, Spraker MB, Prodoehl J, Abraham I, Corcos DM, Zhou XJ, Comella CL, Little DM. High-resolution diffusion tensor imaging in the substantia nigra of de novo Parkinson disease. Neurology 2009;72:1378-84.

Cite this article as: Yu J, Chen L, Cai G, Wang Y, Chen X, Hong W, Ye Q. Evaluating white matter alterations in Parkinson's disease-related *parkin* S/N167 mutation carriers using tract-based spatial statistics. Quant Imaging Med Surg 2022;12(8):4272-4285. doi: 10.21037/qims-21-1007

Supplementary

Table S1 The fiber bundles extracted

No.	X	Y	Z	Name
1	69	83	36	Middle cerebellar peduncle
2	89	97	40	Pontine crossing tract (a part of MCP)
3	93	152	77	Genu of corpus callosum
4	95	100	97	Body of corpus callosum
5	85	89	88	Splenium of corpus callosum
6	89	116	88	Fornix (column and body of fornix)
7	82	103	43	Corticospinal tract R
8	97	103	43	Corticospinal tract L
9	84	89	40	Medial lemniscus R
10	95	89	40	Medial lemniscus L
11	83	83	20	Inferior cerebellar peduncle R
12	96	83	20	Inferior cerebellar peduncle L
13	84	93	53	Superior cerebellar peduncle R
14	95	93	53	Superior cerebellar peduncle L
15	75	107	60	Cerebral peduncle R
16	104	107	60	Cerebral peduncle L
17	75	129	79	Anterior limb of internal capsule R
18	104	129	79	Anterior limb of internal capsule L
19	66	108	85	Posterior limb of internal capsule R
20	113	108	85	Posterior limb of internal capsule L
21	61	101	78	Retrolenticular part of internal capsule R
22	117	101	78	Retrolenticular part of internal capsule L
23	69	163	73	Anterior corona radiata R
24	110	163	73	Anterior corona radiata L
25	63	109	96	Superior corona radiata R
26	116	109	96	Superior corona radiata L
27	64	99	99	Posterior corona radiata R
28	115	99	99	Posterior corona radiata L
29	57	64	73	Posterior thalamic radiation (include optic radiation) R
30	122	64	73	Posterior thalamic radiation (include optic radiation) L
31	48	97	60	Sagittal stratum (include inferior longitidinal fasciculus and inferior fronto-occipital fasciculus) R
32	131	97	60	Sagittal stratum (include inferior longitidinal fasciculus and inferior fronto-occipital fasciculus) L
33	58	131	64	External capsule R
34	121	131	64	External capsule L
35	83	132	105	Cingulum (cingulate gyrus) R
36	97	110	108	Cingulum (cingulate gyrus) L
37	66	101	53	Cingulum (hippocampus) R
38	112	99	54	Cingulum (hippocampus) L
39	62	100	66	Fornix (cres) / Stria terminalis (cannot be resolved with current resolution) R
40	117	100	66	Fornix (cres) / Stria terminalis (cannot be resolved with current resolution) L
41	53	103	102	Superior longitudinal fasciculus R
42	126	103	102	Superior longitudinal fasciculus L
43	69	121	93	Superior fronto-occipital fasciculus (could be a part of anterior internal capsule) R
44	110	121	93	Superior fronto-occipital fasciculus (could be a part of anterior internal capsule) L
45	55	127	54	Uncinate fasciculus R
46	123	125	58	Uncinate fasciculus L
47	60	78	86	Tapetum R
48	117	76	87	Tapetum L

https://dx.doi.org/10.21037/qims-21-1007

Table S2 Demographic and behavioral characteristics of the included participants

	HC		PD		P	
	HC-G/G	HC-G/A	PD-G/G	PD-G/A	P_1	P_2
No. (male)	15 (6)	13 (6)	12 (8)	14 (6)	0.743[d]	0.255[d]
Age	61.9±6.6	62.7±5.5	66.3±6.1	64.8±7.5	0.744[b]	0.574[b]
MMSE	25.8±2.2	25.4±2.9	25.3±2.7	24.7±2.2	0.87[a]	0.436[c]
H-Y	/	/	2.2±0.3	2.5±0.4	/	0.053[c]
UPDRS-III	/	/	30.3±7.7	36.5±9.9	/	0.089[b]

[a], Chi-square test; [b], independent sample *t*-test; [c], Mann-Whitney U test; [d], Fisher's exact probability method. P<0.05 was considered statistically significant. P_1: the significance between HC-G/G and HC-G/A group; P_2: the significance between PD-G/G and PD-G/A group; HC-G/G and HC-G/A respectively refer to the G/G subgroup and G/A subgroup in the HC group; PD-G/G and PD-G/A respectively refer to the G/G subgroup and G/A subgroup in the PD group. G/G-HC and G/G-PD respectively refer to the HC subgroup and PD subgroup in the G/G group. G/A-HC and G/A-PD refer to the HC subgroup and the PD subgroup in the G/A group. HC, Healthy control; PD, Parkinson's disease; G/G, Gene S/N167mutation noncarrier; G/A, Gene S/N167mutation carrier; MMSE, Mini Mental State Scale; H-Y, Hoehn-Yahr Stage scale; UPDRS-III, Unified Parkinson's Disease Rating scale.

Table S3 Comparison of DTI imaging (FA) indices between the healthy controls and the patients with PD

Tracts	HC	PD	Voxel	Coordinate			P	Cohen's d	Cohen's r
				X	Y	Z			
Anterior corona radiata L	0.46±0.04	0.44±0.04	1004	71	158	63	*0.045[a]	0.5	0.24
Anterior corona radiata R	0.51±0.03	0.48±0.04	268	103	138	67	**0.003[a]	0.85	0.39
Anterior limb of internal capsule L	0.53±0.03	0.5±0.04	404	77	138	68	**0.009[a]	0.85	0.39
Anterior limb of internal capsule R	0.58±0.03	0.55±0.04	1085	91	144	89	**0.007[b]	0.85	0.39
Body of corpus callosum	0.44±0.02	0.42±0.03	758	123	115	59	**0.006[a]	0.78	0.37
External capsule L	0.42±0.03	0.4±0.03	328	53	115	59	*0.013[b]	0.67	0.32
External capsule R	0.56±0.03	0.54±0.03	207	122	110	61	**0.008[a]	0.67	0.32
Fornix Stria terminalis L	0.56±0.04	0.54±0.04	92	58	111	61	*0.032[a]	0.57	0.27
Fornix Stria terminalis R	0.65±0.03	0.62±0.04	772	87	155	78	**0.008[a]	0.85	0.39
Genu of corpus callosum	0.44±0.02	0.42±0.03	279	118	85	91	*0.011[a]	0.78	0.37
Posterior corona radiata L	0.42±0.02	0.4±0.03	133	65	101	97	**0.006[a]	0.67	0.32
Posterior corona radiata R	0.58±0.04	0.55±0.04	331	56	65	69	*0.027[a]	0.75	0.35
Posterior thalamic radiation R	0.57±0.02	0.56±0.02	263	127	100	69	*0.017[a]	0.5	0.24
Retrolenticular part of internal capsule L	0.57±0.03	0.55±0.03	301	51	97	69	*0.031[a]	0.67	0.32
Retrolenticular part of internal capsule R	0.59±0.03	0.57±0.03	97	106	82	96	*0.022[a]	0.67	0.32
Splenium of corpus callosum	0.46±0.03	0.44±0.04	342	107	140	102	**0.009[b]	0.57	0.27
Superior corona radiata L	0.44±0.03	0.42±0.04	219	64	109	107	*0.02[a]	0.57	0.27
Superior corona radiata R	0.49±0.02	0.47±0.02	85	120	105	107	***0[a]	1	0.45
Superior longitudinal fasciculus L	0.49±0.02	0.47±0.02	85	120	105	107	***0[a]	1	0.45

[a], independent sample *t*-test; [b], Mann-Whitney U test; *, P<0.05, **, P<0.01,***, P<0.001. L, left; R, right; FA, Fractional anisotropy; HC, Healthy control; PD, Parkinson's disease.

Table S4 Comparison of DTI imaging (MD) indices between the healthy controls and the patients with PD

Tracts	HC ($\times10^{-3}$)	PD ($\times10^{-3}$)	Voxel	Coordinate			P	Cohen's d	Cohen's r
				X	Y	Z			
Posterior corona radiata L	0.78±0.02	0.82±0.05	81	116	96	95	**0.001[a]	1.05	0.46
Posterior corona radiata R	0.82±0.04	0.87±0.07	231	59	80	91	*0.025[b]	0.88	0.4
Posterior thalamic radiation R	0.85±0.04	0.90±0.07	51	59	60	81	*0.002[b]	0.88	0.88
Superior corona radiata L	0.76±0.03	0.79±0.03	190	115	103	97	***0[a]	1	0.45
Superior corona radiata R	0.77±0.03	0.80±0.04	464	65	103	96	**0.001[a]	0.85	0.39
Superior longitudinal fasciculus R	0.74±0.03	0.77±0.038	263	52	86	97	**0.002[a]	0.85	0.39

[a], independent sample *t*-test; [b], Mann-Whitney U test; *, P<0.05, **, P<0.01,***, P<0.001. L, left; R, right; MD, mean diffusivity; HC, Healthy control; PD, Parkinson's disease.

https://dx.doi.org/10.21037/qims-21-1007

Table S5 Comparison of DTI imaging (RD) indices between the healthy controls and the patients with PD

Tracts	HC ($\times10^{-3}$)	PD ($\times10^{-3}$)	Voxel	Coordinate			P	Cohen's d	Cohen's r
				X	Y	Z			
Anterior corona radiata L	0.57±0.04	0.6±0.07	546	109	153	63	*0.025[a]	0.53	0.25
Anterior corona radiata R	0.57±0.05	0.59±0.06	772	74	162	67	0.077[a]	0.36	0.18
Anterior limb of internal capsule L	0.5±0.05	0.56±0.09	262	103	138	67	*0.015[b]	0.82	0.38
Anterior limb of internal capsule R	0.51±0.05	0.56±0.08	358	76	139	68	*0.016[b]	0.75	0.35
Body of corpus callosum	0.56±0.05	0.59±0.06	862	91	144	89	*0.023[a]	0.54	0.26
External capsule L	0.58±0.03	0.61±0.06	781	123	115	59	*0.011[a]	0.63	0.3
External capsule R	0.59±0.05	0.63±0.07	288	62	141	63	*0.038[a]	0.66	0.31
Fornix Stria terminalis L	0.52±0.03	0.55±0.04	91	118	99	66	**0.001[a]	0.85	0.39
Genu of corpus callosum	0.49±0.05	0.53±0.07	698	85	154	79	**0.008[a]	0.66	0.31
Posterior corona radiata L	0.6±0.04	0.63±0.06	409	119	75	91	*0.041[a]	0.59	0.28
Posterior corona radiata R	0.6±0.04	0.63±0.06	300	59	78	91	*0.02[a]	0.59	0.28
Posterior thalamic radiation L	0.54±0.05	0.57±0.06	245	125	67	69	*0.036[a]	0.54	0.26
Posterior thalamic radiation R	0.53±0.04	0.56±0.06	513	56	65	69	*0.014[a]	0.59	0.28
Retrolenticular part of internal capsule L	0.51±0.03	0.53±0.03	183	122	102	69	*0.01[a]	0.67	0.32
Retrolenticular part of internal capsule R	0.54±0.05	0.57±0.05	117	51	95	69	0.075[a]	0.6	0.29
Sagittal stratum L	0.59±0.03	0.61±0.05	82	129	113	58	0.069[a]	0.49	0.24
Splenium of corpus callosum	0.49±0.04	0.51±0.04	100	107	82	96	*0.026[a]	0.5	0.24
Superior corona radiata L	0.56±0.04	0.59±0.04	540	115	105	96	*0.012[a]	0.75	0.35
Superior corona radiata R	0.57±0.03	0.6±0.05	590	65	103	96	**0.007[a]	0.73	0.34
Superior fronto-occipital fasciculus L	0.54±0.05	0.58±0.09	44	112	126	91	0.063[b]	0.55	0.26

[a], independent sample *t*-test; [b], Mann-Whitney U test. *, P<0.05, **, P<0.01. L, left; R, right; RD: radial diffusivity; HC, Healthy control; PD, Parkinson's disease.

https://dx.doi.org/10.21037/qims-21-1007

Table S6 Comparison of DTI imaging (FA) indices between G/A group and G/G group

Tracts	G/G	G/A	Voxel	Coordinate			P	Cohen's d	Cohen's r
				X	Y	Z			
Anterior corona radiata L	0.47±0.03	0.45±0.03	587	104	156	60	**0.01[a]	0.67	0.32
Anterior corona radiata R	0.47±0.04	0.45±0.03	571	70	148	62	*0.024[a]	0.57	0.27
Anterior limb of internal capsule L	0.57±0.03	0.54±0.03	656	103	138	67	***0[a]	1	0.45
Anterior limb of internal capsule R	0.58±0.03	0.56±0.03	556	78	136	68	**0.003[a]	0.67	0.32
Body of corpus callosum	0.61±0.04	0.59±0.03	676	85	96	93	*0.017[a]	0.57	0.27
Cerebral peduncle L	0.7±0.02	0.68±0.02	512	99	96	51	***0[a]	1	0.45
Cerebral peduncle R	0.7±0.02	0.68±0.02	349	78	99	51	***0[a]	1	0.45
Cingulum cingulate gyrus L	0.54±0.04	0.52±0.03	35	100	92	104	*0.032[a]	0.57	0.27
Corticospinal tract L	0.64±0.02	0.62±0.02	82	97	104	41	***0.001[a]	1	0.45
External capsule L	0.46±0.03	0.44±0.02	943	123	115	59	**0.002[a]	0.78	0.37
External capsule R	0.49±0.03	0.47±0.03	411	53	115	59	**0.002[a]	0.67	0.32
Fornix Stria terminalis L	0.56±0.03	0.53±0.03	214	120	112	61	***0.001[a]	1	0.45
Fornix Stria terminalis R	0.53±0.04	0.5±0.03	59	60	97	68	*0.031[a]	0.85	0.39
Genu of corpus callosum	0.69±0.03	0.66±0.03	1413	101	153	64	**0.003[a]	1	0.45
Inferior cerebellar peduncle L	0.51±0.03	0.49±0.03	54	99	77	45	*0.033[a]	0.67	0.32
Inferior cerebellar peduncle R	0.53±0.03	0.5±0.03	65	84	83	21	**0.005[a]	1	0.45
Medial lemniscus L	0.49±0.03	0.47±0.03	30	92	90	28	*0.018[a]	0.67	0.32
Medial lemniscus R	0.6±0.03	0.58±0.03	106	86	91	28	**0.01[a]	0.67	0.32
Middle cerebellar peduncle	0.54±0.02	0.51±0.02	534	65	62	32	***0[a]	1.5	0.6
Pontine crossing tract	0.53±0.04	0.5±0.04	74	85	93	35	*0.025[a]	0.75	0.35
Posterior corona radiata L	0.5±0.03	0.48±0.03	213	118	85	91	**0.008[a]	0.67	0.32
Posterior corona radiata R	0.5±0.03	0.48±0.02	157	60	88	91	*0.011[a]	0.78	0.37
Posterior limb of internal capsule L	0.68±0.02	0.66±0.02	838	110	107	68	***0[a]	0.5	0.24
Posterior limb of internal capsule R	0.67±0.03	0.65±0.02	735	68	107	68	**0.002[a]	0.78	0.37
Posterior thalamic radiation L	0.59±0.03	0.57±0.03	604	125	63	69	**0.007[a]	0.67	0.32
Posterior thalamic radiation R	0.6±0.04	0.58±0.04	294	53	67	69	0.075[a]	0.5	0.24
Retrolenticular part of internal capsule L	0.6±0.02	0.58±0.02	684	129	98	69	***0[a]	1	0.45
Retrolenticular part of internal capsule R	0.58±0.03	0.56±0.02	449	50	88	69	**0.009[a]	0.78	0.37
Sagittal stratum L	0.54±0.02	0.52±0.03	60	128	80	62	**0.01[a]	0.78	0.37
Sagittal stratum R	0.52±0.03	0.5±0.03	397	50	114	56	*0.032[a]	0.67	0.32
Splenium of corpus callosum	0.75±0.02	0.73±0.03	1244	73	84	79	**0.003[a]	0.78	0.37
Superior cerebellar peduncle L	0.64±0.02	0.63±0.02	49	96	92	49	*0.025[a]	0.5	0.24
Superior corona radiata L	0.49±0.03	0.47±0.02	1101	117	103	91	**0.001[a]	0.78	0.37
Superior corona radiata R	0.48±0.03	0.46±0.02	813	63	103	91	**0.004[a]	0.78	0.37
Superior fronto-occipital fasciculus L	0.46±0.05	0.43±0.03	50	112	126	91	0.022[b]	0.73	0.34
Uncinate fasciculus L	0.52±0.04	0.49±0.04	43	125	124	51	*0.03[a]	0.75	0.35
Uncinate fasciculus R	0.53±0.04	0.5±0.03	49	54	126	51	**0.004[a]	0.85	0.39

[a], independent sample *t*-test; [b], Mann-Whitney U test; *, P<0.05, **, P<0.01,***, P<0.001. L, left; R, right; FA, Fractional anisotropy; G/G, Gene S/N167 polymorphism Noncarriers; G/A, Gene S/N167 polymorphism Carriers.

https://dx.doi.org/10.21037/qims-21-1007

Table S7 Comparison of DTI imaging (MD) indices between G/A group and G/G group

Tracts	G/G ($\times10^{-3}$)	G/A ($\times10^{-3}$)	Voxel	Coordinate			P	Cohen's d	Cohen's r
				X	Y	Z			
Anterior corona radiata L	0.77±0.05	0.8±0.04	43	105	146	98	*0.021[a]	0.66	0.31
Anterior limb of internal capsule L	0.73±0.03	0.78±0.06	126	106	143	70	***0[a]	1.05	0.47
Anterior limb of internal capsule R	0.76±0.03	0.79±0.03	31	78	125	72	**0.008	1	0.45
Body of corpus callosum	0.88±0.05	0.93±0.04	138	91	116	97	***0[a]	1.1	0.48
Cerebral peduncle R	0.73±0.03	0.78±0.03	69	78	99	51	***0[a]	1.67	0.64
Corticospinal tract R	0.71±0.03	0.74±0.03	32	79	100	45	***0[a]	1	0.45
External capsule L	0.77±0.04	0.81±0.04	435	124	124	67	**0.005[a]	0.88	0.4
External capsule R	0.78±0.03	0.81±0.05	180	55	118	71	**0.003[b]	0.73	0.34
Fornix Stria terminalis L	0.75±0.03	0.79±0.03	74	118	100	64	***0[a]	1.33	0.55
Fornix Stria terminalis R	0.72±0.02	0.74±0.03	386	109	112	68	**0.002[a]	0.57	0.27
Posterior limb of internal capsule R	0.74±0.03	0.76±0.03	270	76	119	68	**0.004[a]	0.67	0.32
Posterior thalamic radiation L	0.82±0.04	0.86±0.05	200	125	71	69	**0.005[a]	0.88	0.4
Posterior thalamic radiation R	0.81±0.03	0.84±0.05	301	54	62	69	**0.004[b]	0.73	0.34
Retrolenticular part of internal capsule L	0.77±0.02	0.79±0.03	328	126	101	69	**0.001[a]	2.75	0.81
Retrolenticular part of internal capsule R	0.8±0.03	0.82±0.03	95	54	88	79	**0.009[a]	0.67	0.32
Sagittal stratum L	0.82±0.03	0.84±0.04	46	128	79	63	*0.011[a]	0.57	0.27
Sagittal stratum R	0.82±0.03	0.85±0.04	246	46	99	57	*0.024[b]	0.85	0.39
Superior corona radiata L	0.75±0.03	0.77±0.03	366	117	104	91	*0.011[a]	0.67	0.32
Superior corona radiata R	0.75±0.03	0.78±0.03	142	63	104	91	**0.008[a]	1	0.45
Superior longitudinal fasciculus L	0.73±0.02	0.75±0.03	323	124	96	97	**0.003[a]	0.78	0.37
Superior longitudinal fasciculus R	0.75±0.03	0.77±0.03	126	55	94	97	**0.004[b]	0.67	0.32

[a], independent sample *t*-test; [b], Mann-Whitney U test. *, P<0.05, **, P<0.01, ***, P<0.001. L, left; R, right; MD, mean diffusivity; G/G, Gene S/N167 polymorphism Noncarriers; G/A, Gene S/N167 polymorphism Carriers.

https://dx.doi.org/10.21037/qims-21-1007

Table S8 Comparison of DTI imaging (RD) indices between G/A group and G/G group

Tracts	G/G ($\times10^{-3}$)	G/A ($\times10^{-3}$)	Voxel	Coordinate			P	Cohen's d	Cohen's r
				X	Y	Z			
Anterior corona radiata L	0.56±0.05	0.58±0.04	493	103	157	60	0.056[a]	0.44	0.22
Anterior corona radiata R	0.56±0.06	0.59±0.05	256	70	148	62	0.063[a]	0.54	0.26
Anterior limb of internal capsule L	0.47±0.04	0.51±0.04	580	103	138	67	***0[a]	1	0.45
Anterior limb of internal capsule R	0.48±0.04	0.51±0.04	433	78	136	68	**0.004[a]	0.75	0.35
Body of corpus callosum	0.52±0.05	0.55±0.04	481	86	129	96	**0.006[a]	0.66	0.31
Cerebral peduncle L	0.36±0.02	0.4±0.02	426	99	96	51	***0[a]	2	0.71
Cerebral peduncle R	0.38±0.03	0.41±0.02	286	78	99	51	***0[a]	1.18	0.51
Corticospinal tract L	0.4±0.03	0.42±0.03	64	97	104	41	***0[a]	0.67	0.32
Corticospinal tract R	0.38±0.04	0.4±0.03	28	78	101	47	*0.02[a]	0.57	0.27
External capsule L	0.56±0.05	0.59±0.04	944	125	119	59	**0.007[a]	0.66	0.31
External capsule R	0.55±0.04	0.59±0.04	259	55	122	69	**0.002[a]	0.88	0.4
Fornix Stria terminalis L	0.51±0.03	0.55±0.04	151	120	109	62	***0[a]	1.13	0.49
Genu of corpus callosum	0.42±0.05	0.46±0.04	1165	101	153	64	**0.008[a]	0.88	0.4
Inferior cerebellar peduncle R	0.47±0.02	0.49±0.03	52	82	83	26	**0.002[a]	0.78	0.37
Medial lemniscus R	0.44±0.03	0.46±0.02	46	83	86	40	**0.005[a]	0.78	0.37
Middle cerebellar peduncle	0.43±0.02	0.45±0.03	551	59	69	29	**0.001[b]	0.78	0.37
Pontine crossing tract	0.48±0.03	0.5±0.03	56	80	94	39	**0.002[a]	0.67	0.32
Posterior corona radiata L	0.55±0.04	0.58±0.04	177	118	85	91	*0.028[a]	0.75	0.35
Posterior corona radiata R	0.55±0.04	0.57±0.04	133	60	88	91	*0.048[a]	0.5	0.24
Posterior limb of internal capsule L	0.38±0.02	0.41±0.03	819	110	107	68	***0[a]	1.18	0.51
Posterior limb of internal capsule R	0.4±0.03	0.42±0.03	704	68	107	68	**0.003[a]	0.67	0.32
Posterior thalamic radiation L	0.51±0.04	0.54±0.05	466	125	63	69	*0.012[a]	0.66	0.31
Posterior thalamic radiation R	0.51±0.05	0.54±0.05	442	54	62	69	*0.048[b]	0.6	0.29
Retrolenticular part of internal capsule L	0.47±0.03	0.5±0.03	637	127	100	69	***0	1	0.45
Retrolenticular part of internal capsule R	0.5±0.04	0.52±0.03	410	51	88	69	**0.006[a]	0.57	0.27
Sagittal stratum L	0.55±0.03	0.57±0.04	67	128	80	62	*0.014[b]	0.57	0.27
Sagittal stratum R	0.56±0.04	0.58±0.04	396	50	114	56	*0.032[a]	0.5	0.24
Splenium of corpus callosum	0.31±0.04	0.34±0.03	741	72	82	80	**0.004[a]	0.85	0.39
Superior corona radiata L	0.53±0.03	0.56±0.03	1059	117	103	91	**0.003[a]	1	0.45
Superior corona radiata R	0.54±0.04	0.56±0.03	714	63	104	91	**0.007[a]	0.57	0.27
Superior fronto-occipital fasciculus L	0.54±0.08	0.57±0.05	41	112	126	91	*0.02[b]	0.45	0.22
Superior longitudinal fasciculus L	0.52±0.03	0.54±0.03	439	122	128	90	**0.003[a]	0.67	0.32
Superior longitudinal fasciculus R	0.53±0.03	0.56±0.03	318	57	128	90	**0.002[b]	1	0.45
Uncinate fasciculus R	0.51±0.04	0.54±0.05	46	54	126	52	*0.025[b]	0.66	0.31

[a], independent sample *t*-test; [b], Mann-Whitney U test. *, P<0.05, **, P<0.01, ***, P<0.001. L, left; R, right; RD, radial diffusivity; G/G, Gene S/N167 polymorphism Noncarriers; G/A, Gene S/N167 polymorphism Carriers.

https://dx.doi.org/10.21037/qims-21-1007

Table S9 Comparison of DTI imaging (FA) indices between PD- G/A group and PD-G/G group

Tracts	PD-GG	PD-GA	Voxel	Coordinate			P
				X	Y	Z	
Corticospinal tract L	0.5±0.09	0.46±0.05	82	97	104	41	**0.005
External capsule L	0.66±0.05	0.64±0.03	943	123	115	59	*0.036
External capsule R	0.46±0.04	0.43±0.02	411	53	115	59	*0.01
Fornix Stria terminalis L	0.27±0.03	0.25±0.02	214	120	112	61	*0.039
Genu of corpus callosum	0.53±0.04	0.5±0.03	1413	101	153	64	*0.023
Middle cerebellar peduncle	0.59±0.03	0.57±0.02	534	65	62	32	*0.024
Retrolenticular part of internal capsule L	0.59±0.04	0.57±0.04	684	129	98	69	*0.014

Bonferroni tests were used to assess between-group differences; *, P<0.05, **, P<0.01. L, left; R, right; FA, Fractional anisotropy; HC, Healthy control; PD, Parkinson's disease; G/G, Gene S/N167 polymorphism Noncarriers; G/A, Gene S/N167 polymorphism Carriers.

Table S10 Comparison of DTI imaging (MD) indices between PD- G/A group and PD-G/G group

Tracts	PD-GG	PD-GA	Voxel	Coordinate			P
				X	Y	Z	
Anterior limb of internal capsule L	0.74±0.04	0.79±0.06	126	126	106	143	0.053
Corticospinal tract R	0.73±0.04	0.78±0.04	32	32	79	100	*0.023
External capsule L	0.78±0.05	0.82±0.04	435	435	124	124	0.05
Fornix Stria terminalis L	0.75±0.04	0.79±0.04	74	74	118	100	0.011

Bonferroni tests were used to assess between-group differences; *, P<0.05, **, P<0.01. L, left; R, right; MD, mean diffusivity; HC, Healthy control; PD, Parkinson's disease; G/G, Gene S/N167 polymorphism Noncarriers; G/A, Gene S/N167 polymorphism Carriers.

Table S11 Comparison of DTI imaging (RD) indices between PD- G/A group and PD-G/G group

Tracts	PD-GG	PD-GA	Voxel	Coordinate			P
				X	Y	Z	
Anterior limb of internal capsule L	0.47±0.05	0.52±0.05	580	103	138	67	*0.049
Cerebral peduncle L	0.36±0.02	0.4±0.03	426	99	96	51	**0.002
Cerebral peduncle R	0.39±0.03	0.42±0.03	286	78	99	51	*0.048
Corticospinal tract L	0.4±0.03	0.43±0.03	64	97	104	41	**0.008
External capsule R	0.55±0.05	0.59±0.04	259	55	122	69	*0.046
Fornix Stria terminalis L	0.52±0.04	0.56±0.04	151	120	109	62	*0.01
Genu of corpus callosum	0.43±0.05	0.48±0.04	1165	101	153	64	*0.036
Retrolenticular part of internal capsule L	0.47±0.03	0.51±0.02	637	127	100	69	0.023

Bonferroni tests were used to assess between-group differences; *, P<0.05, **, P<0.01. L, left; R, right; RD, radial diffusivity; HC, Healthy control; PD, Parkinson's disease; G/G, Gene S/N167 polymorphism Noncarriers; G/A, Gene S/N167 polymorphism Carriers.

Table S12 Comparison of DTI imaging (FA) indices between HC-G/A group and HC-G/G group

Tracts	HC-GG	HC-GA	Voxel	Coordinate			P
				X	Y	Z	
Anterior corona radiata L	0.48±0.03	0.48±0.03	587	104	156	60	0.564
Cerebral peduncle L	0.7±0.02	0.59±0.02	512	99	96	51	**0.001
Cerebral peduncle R	0.71±0.02	0.67±0.02	349	78	99	51	**0.001
Middle cerebellar peduncle	0.54±0.02	0.59±0.03	534	65	62	32	*0.037
Posterior limb of internal capsule L	0.69±0.02	0.48±0.03	838	110	107	68	**0.004
Posterior limb of internal capsule R	0.68±0.02	0.66±0.02	735	68	107	68	**0.002
Superior corona radiata L	0.49±0.02	0.63±0.03	1101	117	103	91	0.051
Superior corona radiata R	0.48±0.03	0.47±0.02	813	63	103	91	0.071

Bonferroni tests were used to assess between-group differences; *, P<0.05, **, P<0.01. L, left; R, right; FA, Fractional anisotropy; HC, Healthy control; PD, Parkinson's disease; G/G, Gene S/N167 polymorphism Noncarriers; G/A, Gene S/N167 polymorphism Carriers.

https://dx.doi.org/10.21037/qims-21-1007

Table S13 Comparison of DTI imaging (MD) indices between HC-G/A group and HC-G/G group

Tracts	HC-GG	HC-GA	Voxel	Coordinate			P
				X	Y	Z	
Anterior limb of internal capsule L	0.72±0.02	0.77±0.06	126	126	106	143	*0.032
Anterior limb of internal capsule R	0.76±0.02	0.8±0.03	31	31	78	125	*0.027
Body of corpus callosum	0.87±0.05	0.93±0.04	138	138	91	116	*0.013
Corticospinal tract R	0.73±0.03	0.78±0.02	32	32	79	100	**0.004
Superior corona radiata R	0.74±0.01	0.78±0.03	142	142	63	104	0.043

Bonferroni tests were used to assess between-group differences; *, P<0.05, **, P<0.01. L, left; R, right; MD, mean diffusivity; HC, Healthy control; PD, Parkinson's disease; G/G, Gene S/N167 polymorphism Noncarriers; G/A, Gene S/N167 polymorphism Carriers.

Table S14 Comparison of DTI imaging (RD) indices between HC-G/A group and HC-G/G group

Tracts	PD-GG	PD-GA	Voxel	Coordinate			P
				X	Y	Z	
Anterior limb of internal capsule L	0.47±0.05	0.52±0.05	580	103	138	67	*0.049
Cerebral peduncle L	0.36±0.02	0.4±0.03	426	99	96	51	**0.002
Cerebral peduncle R	0.39±0.03	0.42±0.03	286	78	99	51	*0.048
Corticospinal tract L	0.4±0.03	0.43±0.03	64	97	104	41	**0.008
External capsule R	0.55±0.05	0.59±0.04	259	55	122	69	*0.046
Fornix Stria terminalis L	0.52±0.04	0.56±0.04	151	120	109	62	*0.01
Genu of corpus callosum	0.43±0.05	0.48±0.04	1165	101	153	64	*0.036
Retrolenticular part of internal capsule L	0.47±0.03	0.51±0.02	637	127	100	69	0.023

Bonferroni tests were used to assess between-group differences; *, P<0.05, **, P<0.01. L, left; R, right; RD, radial diffusivity; HC, Healthy control; PD, Parkinson's disease; G/G, Gene S/N167 polymorphism Noncarriers; G/A, Gene S/N167 polymorphism Carriers.

https://dx.doi.org/10.21037/qims-21-1007

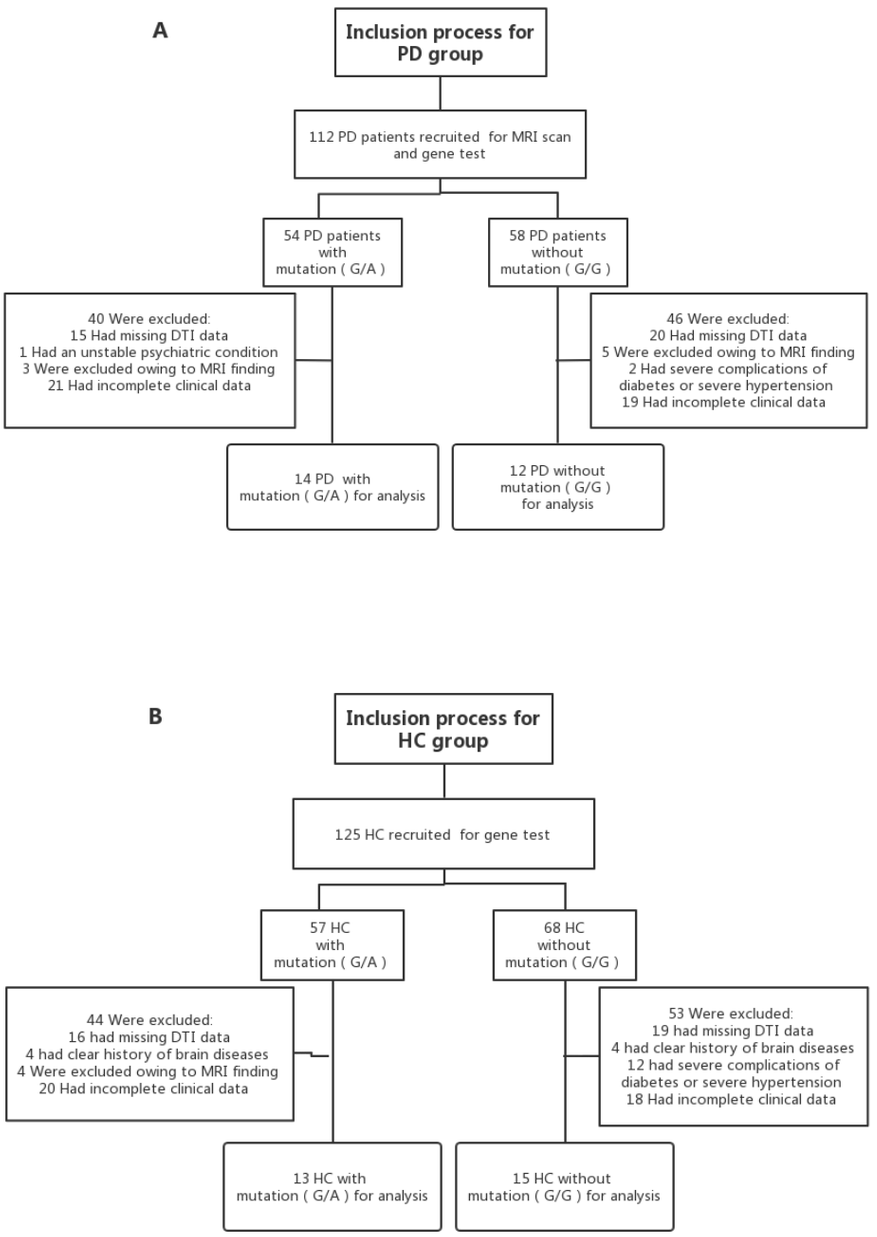

Figure S1 The flow diagram of inclusion process for PD and HC group. (A) The flow diagram of inclusion process for PD group. (B) The flow diagram of inclusion process for HC group. HC, Healthy control; PD, Parkinson's disease; G/G, Gene S/N167 polymorphism noncarriers; G/A, Gene S/N167 polymorphism Carriers.

https://dx.doi.org/10.21037/qims-21-1007